Available online at www.sciencedirect.com

SCIENCE DIRECT

Physics Letters B 633 (2006) 245–252

PHYSICS LETTERS B

www.elsevier.com/locate/physletb

Proton–nucleus scattering and cross section fluctuations at RHIC and LHC

V. Guzey [a,*], M. Strikman [b]

[a] *Institut für Theoretische Physik II, Ruhr-Universität Bochum, D-44780 Bochum, Germany*
[b] *Department of Physics, Pennsylvania State University, University Park, PA 16802, USA*

Received 20 May 2005; received in revised form 20 October 2005; accepted 16 November 2005

Available online 9 December 2005

Editor: J.-P. Blaizot

Abstract

We consider high-energy proton–heavy nucleus scattering within the framework of the Glauber–Gribov approximation and taking into account cross section fluctuations. Fixing parameters of the model for cross section fluctuations by the available data, we make predictions for the total, elastic and coherent diffractive dissociation proton–nucleus cross sections for the RHIC and LHC energy range. We predict a strong change of the A-dependence of diffraction dissociation from $A^{0.42}$ at RHIC energies to $A^{0.27}$ at LHC energies. Based on the obtained results, we discuss the approach of the interactions to the black body (unitarity) limit. We estimate the electromagnetic contribution to coherent pA diffraction and find that it dominates the coherent diffractive cross section on heavy nuclear targets in the LHC kinematics.

PACS: 12.40.-y; 13.85.Lg; 24.10.Jv

1. Introduction

With the advent of the Large Hadron Collider (LHC) one will have an opportunity to study proton–proton, proton–nucleus and nucleus–nucleus collisions at the unprecedentedly high energies, $\sqrt{s} = 14$, 9 and 6 GeV per nucleon, respectively [1]. While the main physics drive of the LHC is the search for Higgs boson, supersymmetry and other physics beyond the Standard Model, many ideas of the traditional physics of soft and hard hadron–hadron interactions can be tested. In particular, one should be able to address the issue of blackening of strong interactions at high energies much better than this can be done at the RHIC and Tevatron energies. In this work, the term *blackening* means the approach of a given partial wave its limiting value given by unitarity of the scattering operator. We refer to this regime the black body limit (BBL). Specifically, the TOTEM Collaboration [2] at the LHC intends to study the total, elastic and diffractive dissociation proton–proton cross sections at the maximal accelerator energy of $\sqrt{s} = 14$ GeV with the aim to test various models, whose predictions depend on the way the BBL is implemented.

It is commonly believed that phenomena associated with high parton densities are more pronounced in nuclei than in free nucleons. In this respect, examining the energy and the atomic mass number A dependence of total, elastic and diffractive dissociation cross sections in hadron–nucleus scattering, one is expected to see an enhancement of the effects related to blackening of the proton–proton interaction.

In this work, we consider total, elastic and diffractive dissociation proton–nucleus cross sections. As a starting point, we use the well-established Glauber–Gribov multiple scattering formalism [3,4], which is known to work with a few percent accuracy for total and elastic hadron–nucleus cross sections. While the Glauber method is essentially based on nonrelativistic quantum mechanics, which takes into account only elastic intermediate states, its generalization by Gribov within the field-theoretical framework also includes inelastic (diffractive) intermediate states. The latter is a manifestation of the increase of the coherence length associated with the given process with energy [5]. A convenient way to model this essential feature of high-energy hadron scattering is by working with eigenstates of the scattering operator and by introducing cross section fluctuations [6–11].

* Corresponding author.
E-mail addresses: vadim.guzey@tp2.ruhr-uni-bochum.de (V. Guzey), strikman@phys.psu.edu (M. Strikman).

0370-2693 © 2005 Elsevier B.V. Open access under CC BY license.
doi:10.1016/j.physletb.2005.11.065

The main goal of the present work is to extend a particular model of cross section fluctuations summarized in [9] to the RHIC and LHC energies and to make predictions for the total, elastic and diffractive dissociation proton–heavy nucleus cross sections and discuss the approach to the black body regime.

2. High-energy hadron–nucleus scattering, Glauber formalism and cross section fluctuations

In order to define and explain the terms "black body (disc) limit", "unitarity", "shadowing" and "diffraction", which we extensively use in this work, it is instructive to consider a simple example of high-energy scattering on a completely absorbing spherical potential with a radius a in non-relativistic quantum mechanics [12]. Making usual partial wave decomposition, one notices that all partial scattering amplitudes with the angular orbital moments $l > l_{\max}$, where $l_{\max} = pa$ and p is the projectile momentum, are zero (no scattering). On the other hand, for the partial scattering amplitudes with $l \leqslant l_{\max}$, scattering is maximal in the sense that there is no transmitted wave (there is a *shadow* formed right behind the target sphere) and, hence, the scattered wave equals minus the incoming wave, i.e. the partial scattering amplitudes are $f_l = i/(2p)$ for $l \leqslant l_{\max}$. Using the optical theorem, one readily finds the total cross section

$$\sigma_{\text{tot}} = 2\pi a^2, \tag{1}$$

which is twice as large as the geometric cross section of the target πa^2. One can separately calculate the elastic cross section with the result $\sigma_{\text{el}} = \pi a^2$ and, hence, the difference between the total and elastic cross sections, the inelastic cross section, is $\sigma_{\text{inel}} = \pi a^2$.

These classic results can be understood by noticing that the completely absorbing potential of radius a serves as a *black body* obstacle in the way of the incoming plane wave and that one deals with *diffraction* of the plane wave on a *black disc*. Then in accordance with Babinet's principle of wave optics, the intensity of the scattered or diffracted light (which is analogous to σ_{el} of our quantum mechanical exercise) is equal to the intensity of light scattered in diffraction on the circular opening of size a in an opaque screen, which is proportional to πa^2. At the same time, the intensity of the absorbed light, which is analogous to σ_{inel}, is also proportional to πa^2, which means that $\sigma_{\text{el}} = \sigma_{\text{inel}} = \pi a^2$. The considered example shows that the formation of a shadow behind the scattering center leads to diffraction. If the scattering potential is a black body, scattering is maximal and the elastic cross section (which is, at the same time, the diffractive cross section) equals half the total cross section. The latter is twice as large as the geometric transverse cross section of the target black disc. A nice discussion of diffraction in high-energy scattering can be found in [13].

In order to show that scattering off the black body is indeed maximal, we recall the general condition on the partial scattering amplitudes, which is a consequence of unitarity of the scattering operator,

$$\text{Im}\, f_l(\theta) = p\big|f_l(\theta)\big|^2 + pG_l^{\text{in}}(\theta), \tag{2}$$

where G_l^{in} accounts for inelastic processes; θ is the scattering angle. Solving Eq. (2) for Im $f_l(\theta)$ and choosing the smaller of the two solutions, we obtain

$$\text{Im}\, f_l(\theta) = \frac{1}{2p}\Big(1 - \sqrt{1 - 4p^2\big(|\,\text{Re}\, f_l|^2 + G_l^{\text{in}}\big)}\Big). \tag{3}$$

From this equation, one sees that the maximal value of Im $f_l(\theta)$ is Im $f_l^{\max}(\theta) = 1/(2p)$, which is exactly the value of the scattering amplitude in the black body scattering problem. One can say that the partial scattering amplitudes for $l \leqslant l_{\max}$ *saturate*. While in the considered simple example blackening of Im f_l leads to the energy-independent total cross section, it is not the case in a more realistic situation. For instance, our analysis will demonstrate that the total proton–nucleus cross section slowly increases with energy regardless that many partial waves reach their constant maximal values.

In a number of models, which discuss saturation in hard processes, one often assumes that the total cross section reaches a fixed maximal value or that partial scattering amplitudes reach constant values smaller than the maximal $1/(2p)$, see e.g. [14].

The choice of the smaller of the two solutions to Eq. (2) is a reflection of the fact that in hadron–hadron scattering, the imaginary part of the scattering amplitude is driven by the inelastic contribution.

Turning to hadron–nucleus scattering, we notice that while the target nucleus can be better approximated by a completely absorbing black disk than the target proton, it is still a poor approximation. A better approach was formulated by Glauber [3]. The target nucleus is approximated by a static collection of nucleon scatterers so that the phase of the elastic scattering amplitude is a sum of the phases accumulated in each projectile–nucleon scattering. This means that if we express the elastic hadron–nucleus scattering amplitude $f_A(\vec{q})$ in terms of the profile function $\Gamma_A(\vec{b})$,

$$f_A(\vec{q}) = \frac{ip}{2\pi}\int d^2\vec{b}\, e^{i\vec{q}\cdot\vec{b}}\Gamma_A(\vec{b}), \tag{4}$$

then $\Gamma_A(\vec{b})$ can be expressed in terms of the elementary hadron–nucleon profile functions $\Gamma(\vec{b})$,

$$\Gamma(\vec{b}) = \frac{1}{ip2\pi}\int d^2\vec{q}\, e^{-i\vec{q}\cdot\vec{b}} f(\vec{q}), \tag{5}$$

integrated with the nuclear ground state wave function $\Psi_A(\vec{r}_1, \vec{r}_2, \ldots, \vec{r}_A)$

$$\Gamma_A(\vec{b}) = \int d^3\vec{r}_1\, d^3\vec{r}_2 \cdots d^3\vec{r}_A \left|\Psi_A(\vec{r}_1, \vec{r}_2, \ldots, \vec{r}_A)\right|^2 \times \left(1 - \prod_{i=1}^{i=A}\big(1 - \Gamma(\vec{b} - \vec{s}_i)\big)\right). \tag{6}$$

Eqs. (4)–(6) assume that at high energies the small momentum transfer $\vec{q}$ is perpendicular to the direction of the beam, i.e. it is a two-dimensional vector. The corresponding conjugated variable is the two-dimensional vector of the impact parameter $\vec{b}$. In Eq. (6), the vectors $\vec{s}_i$ are the transverse components of the position of the nucleons $\vec{r}_i$; $f(\vec{q})$ is the hadron–nucleon scattering amplitude. For sufficiently heavy nuclei ($A > 16$) it is

permissible to neglect the nucleon–nucleon correlations in the ground state nuclear wave function, which means that each nucleon moves in the nucleus independently, and to write

$$\left|\Psi_A(\vec{r}_1,\vec{r}_2,\ldots,\vec{r}_A)\right|^2=\prod_{i=1}^{i=A}\rho_A(\vec{r}_i), \tag{7}$$

where the nucleon distribution $\rho_A(\vec{r})$ is normalized to unity. The parameterization of $\rho_A(\vec{r})$ is detailed in Section 4. Then the nuclear profile function for a heavy nucleus can be presented in the following compact form

$$\Gamma_A(\vec{b})=1-\exp\left(-A\int d^3\vec{r}\,\rho_A(\vec{r})\Gamma(\vec{b}-\vec{s})\right). \tag{8}$$

The elementary profile function is readily calculated using the standard parameterization for the elementary proton–nucleon scattering amplitude

$$f(\vec{q})=\frac{ip\sigma_{\rm tot}(s)(1-i\eta)}{4\pi}e^{-B(s)q^2/2}, \tag{9}$$

where $\sigma_{\rm tot}$ is the energy-dependent total cross section; $B(s)$ is the slope of the amplitude; $\eta=\mathrm{Im}\,f(\vec{q})/\mathrm{Re}\,f(\vec{q})$. In our numerical analysis, we use [11]

$$B(s)=10.5+0.5\ln(s/s_0)\ \mathrm{GeV}^{-2}, \tag{10}$$

where $s_0=25$ GeV; $\eta=\pi/2\times 0.0808=0.127$.

Evaluating $\Gamma(\vec{b}-\vec{s})$ using Eq. (5) and substituting the result in Eq. (8), we obtain the Glauber approximation expression for $\Gamma_A(\vec{b})$

$$\Gamma_A(\vec{b})=1-\exp\bigl(-A/2\sigma_{\rm tot}(s)(1-i\eta)T(b)\bigr), \tag{11}$$

where

$$T(b)=\int dz\,d^2\vec{s}\,\frac{e^{-(\vec{b}-\vec{s})^2/(2B(s))}}{2\pi B(s)}\rho_A\left(\sqrt{|\vec{s}|^2+z^2}\right). \tag{12}$$

In the $B(s)\to 0$ limit, the $T(b)$ function takes a more familiar approximate form, $T(b)=\int dz\,\rho_A(\sqrt{b^2+z^2})$.

It is interesting to point out that the profile function $\Gamma_A(\vec{b})$ plays the role of the partial scattering amplitude and the impact parameter $|\vec{b}|$ plays the role of the orbital momentum l. As a consequence, the unitarity condition is diagonal in $|\vec{b}|$ and reads (compare to Eq. (3))

$$2\,\mathrm{Re}\,\Gamma_A(\vec{b})=\left|\Gamma_A(\vec{b})\right|^2+G^{\rm in}(\vec{b}). \tag{13}$$

The solution to this equation is

$$\mathrm{Re}\,\Gamma_A(\vec{b})=\frac{1-\sqrt{1-(1+\eta_A^2)G^{\rm in}(\vec{b})}}{1+\eta_A^2}, \tag{14}$$

where $\eta_A=\mathrm{Im}\,\Gamma_A(\vec{b})/\mathrm{Re}\,\Gamma_A(\vec{b})$. The maximal value of $\mathrm{Re}\,\Gamma_A(\vec{b})$ is unity (η_A vanishes in the black disc limit), and, therefore, the Glauber approximation expression for $\Gamma_A(\vec{b})$ of Eq. (11) trivially complies with the unitarity constraint of Eq. (13).

The Glauber formalism offers a convenient scheme for the calculation of various observables measured in the hadron–nucleus scattering at high-energies such as the total and elastic cross sections

$$\sigma_{\rm tot}^{hA}(s)=2\int d^2\vec{b}\,\mathrm{Re}\,\Gamma_A(\vec{b}),$$
$$\sigma_{\rm el}^{hA}(s)=\int d^2\vec{b}\left|\Gamma_A(\vec{b})\right|^2. \tag{15}$$

It is important to note that while the nuclear profile function saturates, the scattering cross sections in Eq. (15) grow with energy at large s.

The quantum mechanical expressions of the Glauber formalism imply that coherent diffraction on nuclei consists of only elastic scattering. This contradicts experiments on diffraction dissociation, which showed that the incoming particle can dissociate into states with the same quantum numbers leaving the target nucleus in its ground state. Therefore, the Glauber formalism should be extended to accommodate this experimental fact.

A simple picture of diffractive dissociation was suggested by Feinberg and Pomeranchuk [5] and elaborated on by Good and Walker [6]. One thinks of the incoming wave as a coherent superposition of eigenstates of the scattering operator. Each eigenstate interacts with the target with its own cross section. Since in general these cross sections (eigenvalues) are different, the final state contains not only the initial particle but also other states, which *diffracted into existence*. It is important to note that the formalism of scattering eigenstates is based on the assumption that one can represent scattering as superposition of scattering of the components with different interaction strengths. The use of this assumption and the completeness of the set of scattering states allows to obtain compact formulas. In perturbative QCD, this assumption can be justified for $t\sim 0$ relevant for the scattering off nuclei, while it is not valid for sufficiently large t.

Introducing the probability to interact with a given cross section σ, $P(\sigma,s)$, the expressions for the total and elastic hadron–nucleus cross sections become (compare to Eqs. (15))

$$\sigma_{\rm tot}^{hA}(s)=2\int d\sigma\,P(\sigma)\int d^2\vec{b}\,\mathrm{Re}\,\Gamma_A(\vec{b},\sigma),$$
$$\sigma_{\rm el}^{hA}(s)=\int d^2\vec{b}\left|\int d\sigma\,P(\sigma)\Gamma_A(\vec{b},\sigma)\right|^2. \tag{16}$$

In these equations, the profile function $\Gamma_A(\vec{b},\sigma)$ depends on the eigenvalue σ rather than on the total cross section $\sigma_{\rm tot}^{pp}(s)$,

$$\Gamma_A(\vec{b},\sigma)=1-\exp\bigl(-A/2\sigma(1-i\eta)T(b)\bigr). \tag{17}$$

Therefore, the cross sections in Eq. (16) are sensitive not only to the first moment of $P(\sigma,s)$, $\langle\sigma\rangle(s)=\sigma_{\rm tot}^{hp}(s)$, but also to higher moments $\langle\sigma^k\rangle(s)$.

The motivation to introduce cross section fluctuations is the need for a simple picture of diffractive dissociation. The cross section for coherent diffraction dissociation of hadrons on a nuclear target is found as the difference between the coherent diffraction and elastic cross sections [10],

$$\sigma_{\rm DD}^{hA}(s) = \int d^2\vec{b}\left(\int d\sigma\ P(\sigma,s)\left|\Gamma_A(\vec{b},\sigma)\right|^2 - \left|\int d\sigma\ P(\sigma,s)\Gamma_A(\vec{b},\sigma)\right|^2\right). \quad (18)$$

Since $\sigma_{\rm DD}^{hA}(s)$ is identically zero if cross section fluctuations are absent, $\sigma_{\rm DD}^{hA}(s)$ is the most sensitive observable to cross section fluctuations.

At small impact parameters and large σ, the nuclear profile function saturates, $\Gamma_A(\vec{b},\sigma)\approx 1$, and becomes independent of σ. This leads to vanishing $\sigma_{\rm DD}^{hA}(s)$. Therefore, *cross section fluctuations* indicate how close to the *black body limit* regime one is: the proximity to the blackening regime is indicated by the decreasing size of $\sigma_{\rm DD}^{hA}(s)$. Phenomenologically this fact can be taken into account by modeling $P(\sigma)$ which becomes narrower as $\sqrt{s}$ increases and by taking into account the increase of $\sigma_{\rm tot}^{hp}(s)$ with energy, see Fig. 1.

3. Energy dependence of $P(\sigma, s)$

The distribution over cross sections $P(\sigma,s)$ has the following properties [9]:

$$\int_0^\infty d\sigma\ P(\sigma,s) = 1,$$

$$\int_0^\infty d\sigma\ \sigma P(\sigma,s) = \sigma_{\rm tot}(s),$$

$$\int_0^\infty d\sigma\ \sigma^2 P(\sigma,s) = \langle\sigma^2\rangle(s) = \sigma_{\rm tot}^2(s)\big(1+\omega_\sigma(s)\big). \quad (19)$$

The first equation is probability conservation; the second equation requires that $P(\sigma,s)$ reproduces correctly the total hadron–nucleon cross section; the third equation introduces $\omega_\sigma(s)$ which measures the broadness of cross section fluctuations around the average value. One can also consider higher moments of $P(\sigma,s)$.

Eqs. (19) constitute the minimal set of constraints on $P(\sigma,s)$ and one can successfully model $P(\sigma,s)$ using only these constraints and the behavior of $P(\sigma,s)$ in the limiting cases of $\sigma\to 0$ and $\sigma\to\infty$. The constituent quark counting rules suggest that $P(\sigma)=\mathcal{O}(\sigma)$ as $\sigma\to 0$. In addition, convergence of integrals for the moments of $P(\sigma,s)$ (see Eqs. (19)) requires that $P(\sigma,s)\to 0$ faster than any power of σ as $\sigma\to\infty$.

We assume a particular parameterization of $P(\sigma,s)$ [9] and determine free parameters of the parameterization using Eqs. (19) with $\sigma_{\rm tot}(s)$ and ω_σ as an input at each energy. In particular, we use the following form for the proton $P(\sigma,s)$,

$$P(\sigma,s) = N(s)\frac{\sigma}{\sigma+\sigma_0(s)}\exp\left(-\frac{(\sigma/\sigma_0(s)-1)^2}{\Omega^2(s)}\right), \quad (20)$$

whose parameters at typical energies are summarized in Table 1.

It is worth emphasizing that for large $\sigma_{\rm tot}^{hN}$ and for the nuclear observables considered in this Letter, effects of fluctuations are primarily determined by the second moment of $P(\sigma,s)$, i.e. by the value of the dispersion ω_σ [10]. This allows us to use a simple form of $P(\sigma,s)$ with energy-dependent parameters, which still captures the essential features of the distribution over cross sections.

Table 1
Parameters $P(\sigma,s)$ at various typical energies

$\sqrt{s}$, GeV	ω_σ	$\Omega(s)$	$\sigma_0(s)$, mb
24 (nD data, [18])	0.29	2.2	19
61 (pD data, [19])	0.33	3.4	16
546 (UA4, [20])	0.19	0.94	48
546 (CDF, [21])	0.16	0.77	51
1800 (CDF, [21])	0.15	0.72	63
9000 (LHC, pA)	0.10	0.52	88
14 000 (LHC, pp [22])	0.065	0.39	97.5

The total proton–proton cross section $\sigma_{\rm tot}^{pp}(s)$ is calculated using the Regge theory motivated fit by Donnachie and Landshoff [15],

$$\sigma_{\rm tot}^{pp}(s) = 21.7 s^{0.0808} + 56.08 s^{-0.4525}, \quad (21)$$

which is in a good agreement with the available data. Recently more elaborate parameterizations of the total proton–proton cross section, which explicitly implement Froissart's unitarity bound, were suggested [16,17]. An inspection shows that all parameterizations predict the values of the total proton–proton cross section, which differ by 5–10% at the Fermilab and LHC energies. The nuclear cross sections, which we consider, are virtually insensitive to such small differences, primarily due to the approximate saturation of the nuclear profile function $\Gamma_A(\vec{b},\sigma)$, see the discussion in the end of Section 2. We explicitly checked that all nuclear cross sections presented in our work change by at most 1.5%, when instead of the parameterization of $\sigma_{\rm tot}^{pp}(s)$ of Donnachie and Landshoff [15], we use the parameterization of [16]. For the parameterization of [17], the change is absolutely negligible.

The parameter ω_σ is a key input of our analysis since it defines the broadness of $P(\sigma,s)$ ($\omega_\sigma\propto\Omega(s)$) and, hence, the magnitude of cross section fluctuations. Information on ω_σ can be extracted either from the inelastic shadowing correction in proton (neutron)–deuterium total cross section or from proton–proton or proton–antiproton single diffraction at $t=0$, see the details in [9]. For the lower values of $\sqrt{s}$ and the UA4 point at $\sqrt{s}=546$ GeV, we used the results of [9]. In particular, there were used the neutron–deuterium total cross section data [18] (with maximal $\sqrt{s}\approx 24$ GeV), the analysis of [19] of the proton–deuterium data with maximal $\sqrt{s}\approx 61$ GeV), and the proton–antiproton single diffraction data taken by the UA4 experiment at the SPS collider at CERN with $\sqrt{s}=546$ GeV [20].

In addition to this, we used the CDF (Fermilab) data on proton–antiproton single diffraction with $\sqrt{s}=546$ GeV and $\sqrt{s}=1800$ GeV [21]. An extrapolation to the LHC proton–proton energy $\sqrt{s}=14$ TeV, $\omega_s=0.06$–0.07, is done using K. Goulianos fit and is cited in [22]. A linear interpolation between the $\sqrt{s}=1.8$ TeV and $\sqrt{s}=14$ TeV gives an estimate for

the value of ω_s at the proton–nucleus LHC energies, $\omega_s \approx 0.10$. Note that the uncertainty of the extrapolation of diffraction from the Fermilab to the LHC energies (the uncertainty in the value of ω_s) constitutes the main uncertainty of our predictions for the absolute value of $\sigma_{\rm DD}^{hA}$, but it affects only very weakly our predictions for the A-dependence of the diffractive cross section. This uncertainty will be rectified during early runs of the LHC by the pp experiments which will measure diffraction in pp scattering at small t.

It is important to note that judging by the values of ω_σ at $\sqrt{s} = 61$ GeV and $\sqrt{s} = 546$ GeV, the function ω_σ reaches its (broad) maximum around the present RHIC energy range of $\sqrt{s} = 200$ GeV. In our analysis, we assumed that $\omega_\sigma(\sqrt{s} = 200\ \text{GeV}) = 0.3$.

Fig. 1 shows the distribution $P(\sigma, s)$ as a function of σ at three energies considered in Table 1: the solid curve corresponds to $\sqrt{s} = 9$ TeV (pA collisions at the LHC); the dashed curve corresponds to $\sqrt{s} = 1.8$ TeV (Tevatron); the dot-dashed curve corresponds to $\sqrt{s} = 200$ GeV (RHIC). As $\sqrt{s}$ increases, the position of the maximum of $P(\sigma, s)$ increases, which naturally corresponds to the increasing $\sigma_{\rm tot}^{pp}(s)$. Although the dispersion ω_σ becomes progressively smaller as the energy increases, there is no significant change in the width of the distribution as measured by the range of values of σ, where $P(\sigma, s) > 0.5 \max P(\sigma, s)$. Consequently, even at the LHC one should expect significant fluctuations in the number of wounded nucleons in pA scattering at central impact parameters [23].

While the average total cross section increases with energy according to Eq. (21), small cross sections can grow with $\sqrt{s}$ much faster. For instance, the cross sections corresponding to $P(\sigma, s) = 0.002$ in Fig. 1 increase with energy as $\sigma \propto s^{0.5\text{–}0.75}$.

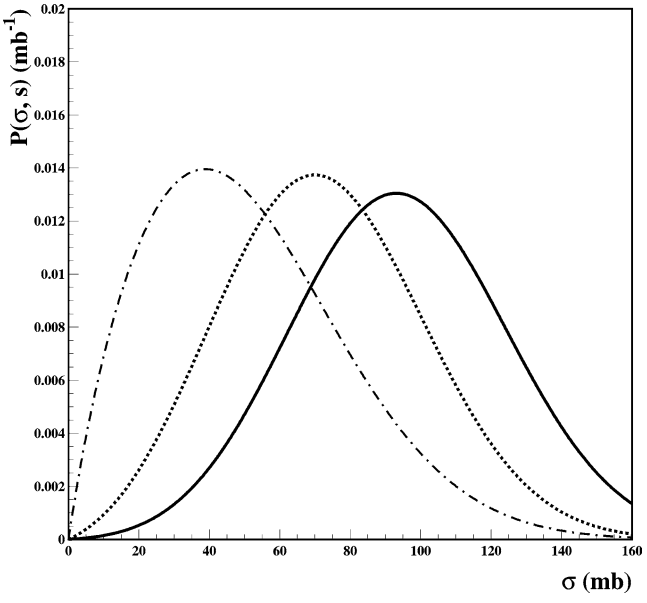

Fig. 1. The cross section distribution $P(\sigma, s)$ at different energies: the solid curve corresponds to $\sqrt{s} = 9$ TeV (LHC); the dashed curve corresponds to $\sqrt{s} = 1.8$ TeV (Tevatron); the dot-dashed curve corresponds to $\sqrt{s} = 200$ GeV (RHIC).

4. Results and discussion

Using Eqs. (15) and (18), we calculate the total, elastic and diffractive dissociation cross sections for proton-^{208}Pb scattering as a function of $\sqrt{s}$. The result is given in Fig. 2.

In our numerical analysis, we used the following parameterization of the nucleon distribution $\rho_A(\vec{r}\,)$

$$\rho_A(\vec{r}\,) = \frac{\rho_0}{1 + \exp((r - c)/a)}, \tag{22}$$

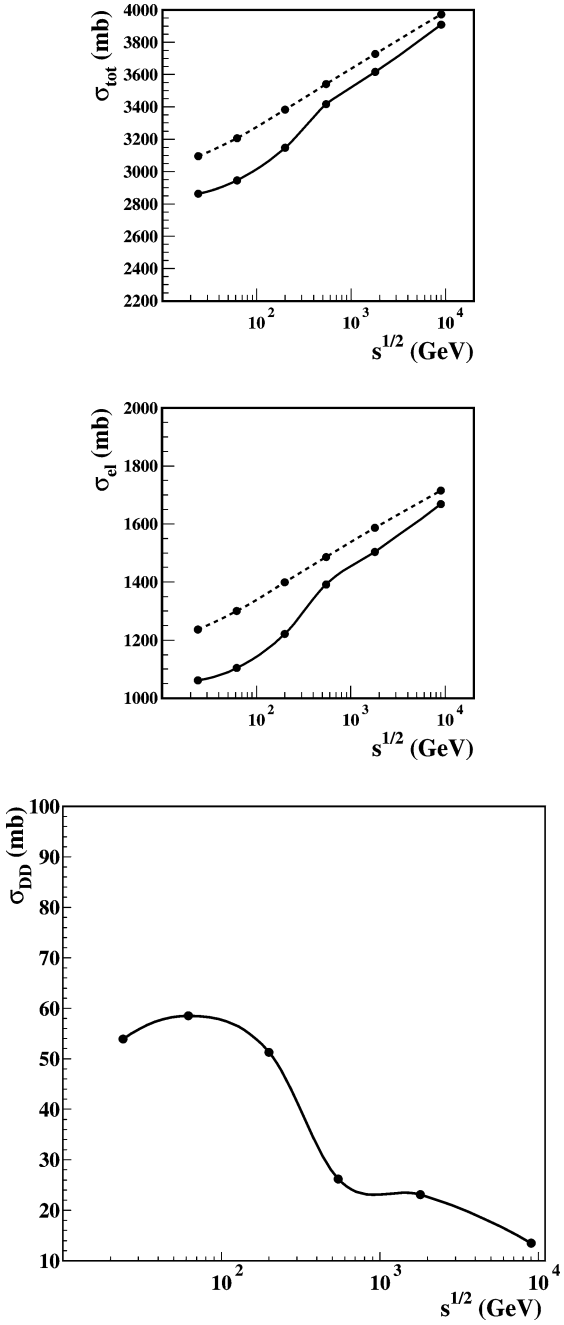

Fig. 2. The proton–lead total, elastic and diffractive dissociation cross sections as functions of $\sqrt{s}$. The solid curves correspond to Glauber formalism with cross section fluctuations; the dashed curves neglect the cross section fluctuations.

where $c = R_A - (\pi a)^2/(3R_A)$ with $R_A = 1.145A^{1/3}$ fm and $a = 0.545$ fm; the constant ρ_0 is chosen to provide the normalization of $\rho_A(\vec{r}\,)$ to unity.

One sees from Fig. 2 that cross section fluctuations decrease the total and elastic cross sections. The effect is largest in the $\sqrt{s} = 100$–200 GeV region. This can be explained by the increasing role of nuclear shadowing: an increase of ω_σ leads to an increase of the inelastic shadowing correction, which decreases the total cross section.

An examination of Fig. 2 shows that, for $\sqrt{s} > 546$ GeV, the total cross section behaves as

$$\sigma_{\rm tot}^{pA}(s) \propto s^{0.045}, \tag{23}$$

which is slower than the input $\sigma_{\rm tot}^{pp}(s) \propto s^{0.0808}$.

The diffractive dissociation cross section (the lower panel of Fig. 2) noticeably decreases with increasing energies for $\sqrt{s} > 200$ GeV. We would like to stress that the predicted diffractive dissociation cross section primarily depends on the input ω_σ [10] and depends only weakly on the shape of the distribution $P(\sigma, s)$. Therefore, the diffractive dissociation cross section is a sensitive tool to study the role of cross section fluctuations.

We also examined the dependence of the total, elastic and diffractive dissociation cross sections at $\sqrt{s} = 200$ GeV (RHIC) and $\sqrt{s} = 9000$ GeV (pA at the LHC) on the atomic number A. The results are summarized in Fig. 3, where the dashed curves correspond to $\sqrt{s} = 200$ GeV and the solid curves correspond to $\sqrt{s} = 9$ TeV.

The total cross section behaves with an increasing atomic number as

$$\begin{aligned} &\sigma_{\rm tot}^{pA} \propto A^{0.70} \quad \text{RHIC}, \\ &\sigma_{\rm tot}^{pA} \propto A^{0.62} \quad \text{LHC}. \end{aligned} \tag{24}$$

The dependence on the atomic number of the diffractive dissociation cross section is much slower

$$\begin{aligned} &\sigma_{\rm DD}^{pA} \propto A^{0.42} \quad \text{RHIC}, \\ &\sigma_{\rm DD}^{pA} \propto A^{0.27} \quad \text{LHC}. \end{aligned} \tag{25}$$

The $\sigma_{\rm DD}^{pA} \propto A^{0.27}$ behavior at the LHC kinematics is slower than the $\sigma_{\rm DD}^{pA} \propto A^{0.4}$ result of [10] at much lower energies: cross section fluctuations play a progressively smaller role as one increases the energy.

It was pointed out in [10] that the fluctuations near the average give the major contribution to $\sigma_{\rm DD}^{hA}$. This point was illustrated by Taylor-expanding the integrand in Eq. (18) about $\sigma = \langle\sigma\rangle$ and keeping only first two non-vanishing terms. The approximate expression for $\sigma_{\rm DD}^{hA}$ reads [10]

$$\sigma_{\rm DD}^{hA} \approx \frac{\omega_\sigma(s)\sigma_{\rm tot}^2(s)}{4} \int d^2\vec{b}\,\big(AT(b)\big)^2 e^{-A\sigma_{\rm tot}(s)T(b)}. \tag{26}$$

Note that the effects of η are small and can be neglected. We would like to emphasize that the integral in Eq. (26) is a smooth function of b, which does not contain a subtraction of two large factors, as appears from Eq. (18). Therefore, $\sigma_{\rm DD}^{hA}$ is much more sensitive to the first moments of $P(\sigma)$, i.e. to $\sigma_{\rm tot}(s)$ and $\omega_\sigma(s)$, rather than to the details of the shape of $P(\sigma)$.

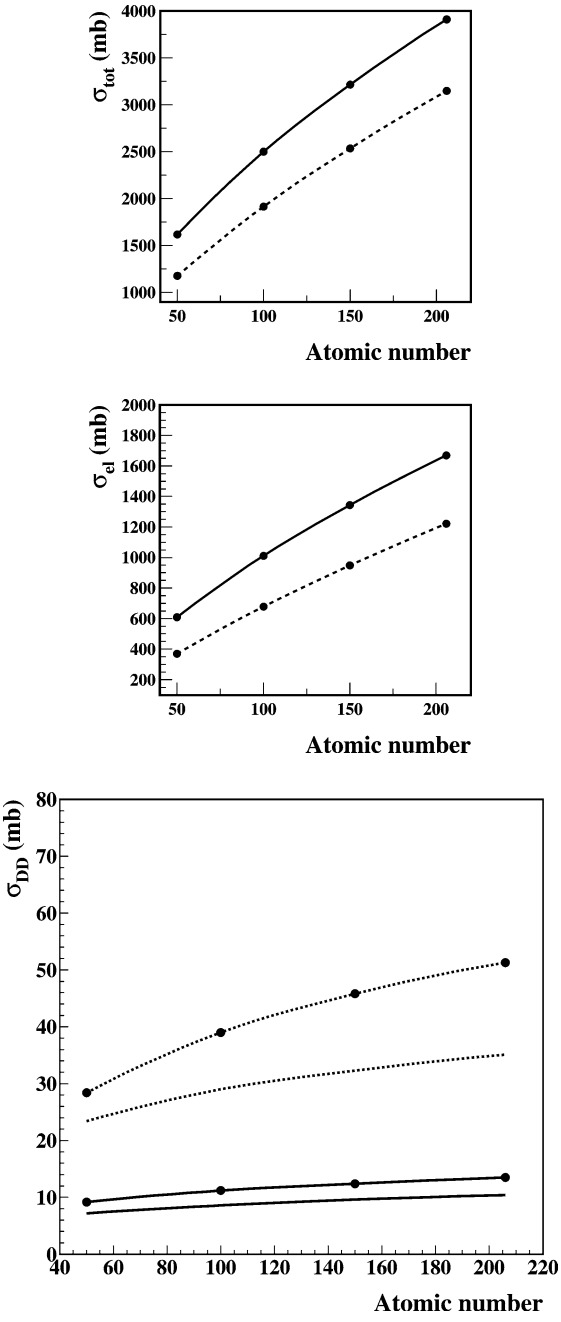

Fig. 3. The atomic number dependence of the total, elastic and diffractive dissociation cross sections. The dashed curves correspond to $\sqrt{s} = 200$ GeV and the solid curves correspond to $\sqrt{s} = 9$ TeV. The second set of dashed and solid curves, which do not go through the points, correspond to the approximate calculation of $\sigma_{\rm DD}$ using Eq. (26).

Calculations of $\sigma_{\rm DD}^{pA}$ using Eq. (26) are presented in the lower panel of Fig. 3 by the second set of dashed and solid curves, which do not go through the points. For the LHC energy, the approximation of Eq. (26) works rather well. For the RHIC energy, the approximation of Eq. (26) is good only qualitatively.

5. Electromagnetic contribution

Coherent pA diffraction, $p + A \to X + A$, has an important electromagnetic contribution originating from the ultraperipheral pA scattering, when the nucleus acts as a source of quasi-real photons which interact with the proton [24]. The smallness of the electromagnetic coupling constant is compensated by nuclear coherence, which gives the enhancement factor Z^2, where Z is the nuclear charge. Therefore, the electromagnetic background becomes important for such heavy nuclei as ^{208}Pb and constitutes a correction for light nuclei down to ^{40}Ca.

Since the strong amplitude is imaginary and the electromagnetic one is real, the two contributions do not interfere. Thus, the cross section of this process is given by convolution of the flux of the equivalent photons, $n(\omega)$, with the photon–proton cross section, $\sigma_{\gamma p}(\omega)$, see e.g. [24]

$$\sigma_{\text{e.m.}}^{pA} = \int_{\omega_{\min}}^{\omega_{\max}} \frac{d\omega}{\omega} n(\omega) \sigma_{\text{tot}}^{\gamma p}(\omega). \tag{27}$$

In this equation,

$$n(\omega) \approx \frac{2Z^2\alpha}{\pi} \ln\left(\frac{\gamma}{\omega R}\right), \tag{28}$$

where γ is the Lorentz factor and R is an effective radius of the nucleus; $\omega_{\max} \approx \gamma/R$; $\omega_{\min}$ determines the minimal photon energy required to excite an inelastic final state. Assuming that the lightest inelastic final state in the γp scattering is $\Delta(1232)$, we obtain $\omega_{\min} = 0.3$ GeV.

In our numerical analysis of Eq. (27), we used $\gamma \approx p_l/m_N$, where p_l is the momentum of the nucleus in the laboratory frame. This corresponds to $\gamma \approx 100$ for RHIC and $\gamma \approx 3000$ for the LHC. The nuclear effective radius was estimated as $R = R_A = 1.145A^{1/3}$ fm, see Eq. (22). The real photon–proton cross section was parameterized in the two-Reggeon form of Donnachie and Landshoff [15],

$$\sigma_{\text{tot}}^{\gamma p}(s) = 0.0677 s^{0.0808} + 0.129 s^{-0.4525}, \tag{29}$$

where $s = 2\omega m_p + m_p^2$.

The resulting electromagnetic contributions to the coherent diffractive cross section are presented in Fig. 4 by dashed curves. They should be compared to the coherent diffractive dissociation cross sections presented by the solid curves. The comparison shows that the electromagnetic contribution completely dominates coherent pA diffraction on Pb-208 in the LHC kinematics, but it becomes smaller than $\sigma_{\text{DD}}^{p\text{Pb}}$ towards the RHIC energies. For the lighter nucleus of Ca-40, the role of the electromagnetic contribution is dramatically reduced: $\sigma_{\text{e.m.}}^{p\text{Ca}}$ is about half of $\sigma_{\text{DD}}^{p\text{Ca}}$ in the LHC kinematics and can be neglected in the RHIC kinematics.

6. Conclusions and discussion

We calculated the total, elastic and diffractive dissociation proton–nucleus cross sections at high energies using the Glauber–Gribov formalism and taking into account inelastic intermediate states by means of the notion of cross section fluctuations. We extended the model of cross section fluctuations of [9] to the RHIC and LHC energies and applied it to the calculation of the cross sections. As a consequence of the decrease of cross section fluctuations at the LHC energy, we observed a significant reduction of the diffractive dissociation cross section in pA coherent diffraction. This calculation can serve as a benchmark calculation, whose comparison to the future data can give information on blackening of the proton–proton interaction.

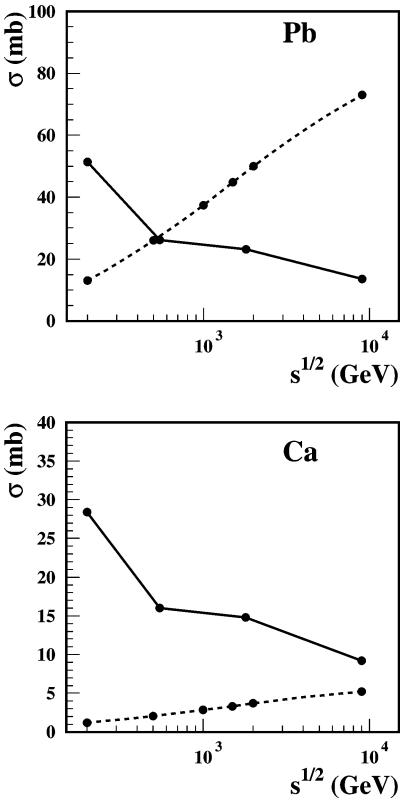

Fig. 4. The electromagnetic contribution evaluated using Eq. (27) (dashed curves) and coherent diffractive dissociation cross sections (solid curves) as functions of $\sqrt{s}$ for Pb and Ca.

We found that towards the LHC energies, $\sqrt{s} = 9$ TeV, $\sigma_{\text{tot}}^{pA} \propto s^{0.045}$, which is slower than the input $\sigma_{\text{tot}}^{pp} \propto s^{0.0808}$. Studying the cross sections as a function of the atomic number A, we found that $\sigma_{\text{tot}}^{pA} \propto A^{0.70}$ and $\sigma_{\text{DD}}^{pA} \propto A^{0.42}$ at $\sqrt{s} =$ 200 GeV (RHIC) and that $\sigma_{\text{tot}}^{pA} \propto A^{0.62}$ and $\sigma_{\text{DD}}^{pA} \propto A^{0.27}$ at $\sqrt{s} = 9$ TeV (LHC).

Another novel result of the present work is an estimate of the electromagnetic contribution to coherent pA diffraction coming from ultraperipheral pA scattering. The electromagnetic smallness of the background is compensated by nuclear coherence (the enhancement factor is proportional to Z^2, where Z is the nuclear charge) and the Lorentz γ factor. We show that when the nuclear momentum in the laboratory frame is large, the ultraperipheral e.m. background completely dominates coherent pA diffraction on Pb in the LHC kinematics, see Fig. 4. One way to reduce the electromagnetic contribution is to use lighter nuclei, such as for example Ca-40.

Acknowledgements

The work is supported by the Sofia Kovalevskaya Program of the Alexander von Humboldt Foundation (Germany) and DOE (USA).

References

[1] A. Acardi, et al., Hard probes in heavy ion collisions at the LHC: PDFs, shadowing and pA collisions, in: Subgroup report of 3rd Workshop on Hard Probes in Heavy Ion Collisions: 3rd Plenary Meeting, Geneva, Switzerland, 7–11 October 2002, hep-ph/0308248.
[2] TOTEM Collaboration, Total cross section, elastic scattering and diffraction dissociation at the LHC, CERN/LHCC 97-49, August 1997.
[3] R.J. Glauber, Phys. Rev. 100 (1955) 242;
V. Franco, Phys. Rev. Lett. 24 (1970) 1452.
[4] V.N. Gribov, Sov. Phys. JETP 29 (1969) 483, Zh. Eksp. Teor. Fiz. 56 (1969) 892.
[5] E.L. Feinberg, I.Ia. Pomeranchuk, Suppl. Nuovo Cimento III (1956) 652.
[6] M.L. Good, W.D. Walker, Phys. Rev. 120 (1960) 1857.
[7] H.I. Miettininen, J. Pumplin, Phys. Rev. D 18 (1978) 1696.
[8] B.Z. Kopeliovich, L.I. Lapidus, A.B. Zamolodchikov, JETP Lett. 33 (1981) 595, Pis'ma Zh. Eksp. Teor. Fiz. 33 (1981) 612.
[9] B. Blättel, G. Baym, L.L. Frankfurt, H. Heiselberg, M. Strikman, Phys. Rev. D 47 (1993) 2761.
[10] L. Frankfurt, G.A. Miller, M. Strikman, Phys. Rev. Lett. 71 (1993) 2859.
[11] M. Strikman, V. Guzey, Phys. Rev. C 52 (1995) 1189.
[12] L.D. Landau, E.M. Lifshitz, Non-Relativistic Quantum Mechanics, second ed., in: Course in Theoretical Physics, vol. 3, Pergamon Press, 1977.
[13] G. Alberi, G. Goggi, Phys. Rep. 74 (1981) 1.
[14] K. Golec-Biernat, M. Wusthoff, Phys. Rev. D 59 (1999) 014017.
[15] A. Donnachie, P.V. Landshoff, Phys. Lett. B 296 (1992) 227.
[16] J.R. Cudell, et al., Phys. Rev. D 65 (2002) 074024.
[17] M.M. Block, F. Halzen, Phys. Rev. D 72 (2005) 036006;
M.M. Block, F. Halzen, Phys. Rev. D 72 (2005) 039902, Erratum.
[18] P.V.R. Murthy, et al., Nucl. Phys. B 92 (1975) 269.
[19] L.G. Dakhno, Sov. J. Nucl. Phys. 37 (1983) 590, Yad. Fiz. 37 (1983) 993.
[20] D. Bernard, et al., UA4 Collaboration, Phys. Lett. B 186 (1987) 227.
[21] F. Abe, et al., CDF Collaboration, Phys. Rev. D 50 (1994) 5535.
[22] A. Ageev, et al., J. Phys. G: Nucl. Part. Phys. 28 (2002) R117.
[23] G. Baym, B. Blättel, L.L. Frankfurt, H. Heiselberg, M. Strikman, Phys. Rev. C 52 (1995) 1604.
[24] G. Baur, K. Hencken, D. Trautmann, S. Sadovsky, Y. Kharlov, Phys. Rep. 364 (2002) 359, hep-ph/0112211.